Journal of Inorganic and General Chemistry
ZAAC
Zeitschrift für anorganische und allgemeine Chemie
www.zaac.wiley-vch.de
RESEARCH ARTICLE

DOI: 10.1002/zaac.202200253

$Li_{16}Sr_6Ge_6N$, $Li_{16}Sr_6Ge_{6.5}$ and related lithium alkaline-earth metal tetrelides: Alternative filling of voids by nitride or tetrelide ions

Peter Höhn,*[a] Manisha Pathak,[a] Yurii Prots,[a] Alexander Ovchinnikov,[a, c] Marcus Schmidt,[a] Matej Bobnar,[a, d] Mitja Krnel,[a] Alim Ormeci,[a] and Rainer Niewa*[b]

Dedicated to Professor Dr. Thomas Schleid on the occasion of his 65th birthday.

Large black single crystals with a metallic luster of $Li_{16}Sr_6Ge_6N$ and several other representatives of the series $Li_{16}AE_6T_6N$ and $Li_{16}AE_6T_{6.5}$ (AE = Ca, Sr; T = Si, Ge, Sn, Pb) were grown from mixtures of the respective elements with addition of binary alkaline-earth metal nitrides or lithium nitride in the case of the nitrides. For the synthesis a modified high-temperature centrifugation-aided filtration (HTCAF) technique using reactive lithium melts was employed. These metallic phases crystallize in an ordered defect-variant of the $Sc_{11}Ir_4$ type with selective occupation of the smaller octahedral voids in the origin (000) with N and the larger rhombic dodecahedral voids in ($00^1/_2$) with T. Charge balance assuming the presence of exclusively closed shell ions for all examples accounts for an electronic excess. Diamagnetism despite metallic properties is consistent with results from electronic structure calculations.

Introduction

In complex nitridometalate ions, exclusively silicon and germanium in oxidation states +4, +3 and +2 have been observed until now. Silicon in nitridosilicates(IV) is always coordinated tetrahedrally by nitrogen like in the famous $Sr_2Si_5N_8$.[1–2] However, nitridogermanate(IV) ions generally feature Ge in tetrahedral $[Ge^{IV}N_{4/x}]^{y-}$ (e.g. $Sr_4[GeN_4]$, $Li_4Sr_3[Ge_2N_6]$)[3,4] or trigonal planar $[Ge^{IV}N_3]^{5-}$ (e.g. $Sr_{17}[Ge]_2[GeN_3]_2[GeN_4]_2$)[3] coordination by nitrogen forming complex networks of different dimensionalities. In nitridogermanates(III), additional direct Ge–Ge interactions are observed in $Sr_6[Ge_2N_6]$ with Ge in a tetrahedral coordination by one further Ge and three N atoms.[5] Two-fold, bent $[Ge^{II}N_2]^{4-}$ coordination is observed in nitridogermanates(II) (e.g. $Sr_2[GeN_2]$);[6] some of these phases may be classified as nitridogermanate-germanides containing also metalide anions.[3] For tin, with NaSnN only one example of a nitridostannate(II) is known,[7] while lead rather forms plumbides.

In metalide nitrides and metalide nitridometalates, the complex anionic substructures are separated by the cations. Isolated metalide ions are observed in the inverse perovskite $(Sr_3N_{0.67})[Ge]$,[8–9] and $Sr_{17}[Ge]_2[GeN_3]_2[GeN_4]_2$,[3] and infinite zigzag chains in e.g. $Sr_6[Ge_4][GeN_2]$.[6] Isolated (non-covalent bonded) nitride ions in metalide nitrides are typically located in octahedra formed by alkaline-earth metal ions. Depending on composition, condensation of these polyhedra (NAE_6) leads to networks of different dimensionality by sharing common vertices, edges, or faces. Nitride metalides containing both Li and AE as well as T and N have not been described yet. Intermetallic phases containing Li, AE, and T are plenty such as Li_2BaSn are numerous.[10] They typically obey the Zintl-rules; and only few phases with excess electrons like Li_5Sn have been reported.[11]

In most of the phases discussed above, both complex anions and metalide ions can be described on the basis of the extended Zintl-Klemm-concept.[12] However, the presumed electron transfer from cations to anions in these phases may be sometimes overstated and both interactions between the cationic and anionic parts of these structures and mixing of states may play an important role in stabilizing these phases,[13] resulting in rather unexpected properties like metallic behavior in $Ca_7N_4[Ga_{1.33}]$.[14]

In this contribution, we demonstrate that depending on whether nitrogen is offered within the starting mixture, either

[a] Dr. P. Höhn, M. Pathak, Dr. Y. Prots, Dr. A. Ovchinnikov, Dr. M. Schmidt, Dr. M. Bobnar, Dr. M. Krnel, Dr. A. Ormeci
Chemische Metallkunde
Max-Planck-Institut für Chemische Physik fester Stoffe
Nöthnitzer Str. 40, 01187 Dresden, Deutschland
E-mail: Peter.Hoehn@cpfs.mpg.de
[b] Prof. Dr. R. Niewa
Institut für Anorganische Chemie
Universität Stuttgart
Pfaffenwaldring 55, 70569 Stuttgart, Deutschland
E-mail: rainer.niewa@iac.uni-stuttgart.de
[c] Dr. A. Ovchinnikov
Department of materials and environmental chemistry
Stockholm University
Svante Arrhenius väg 16 C, 10691 Stockholm, Sweden
[d] Dr. M. Bobnar
Jožef Stefan Institute
Jamova cesta 39, 1000 Ljubljana, Slovenia

Supporting information for this article is available on the WWW under https://doi.org/10.1002/zaac.202200253

© 2022 The Authors. Zeitschrift für anorganische und allgemeine Chemie published by Wiley-VCH GmbH. This is an open access article under the terms of the Creative Commons Attribution License, which permits use, distribution and reproduction in any medium, provided the original work is properly cited.

 © 2022 The Authors. Zeitschrift für anorganische und allgemeine Chemie published by Wiley-VCH GmbH

metalide nitrides or intermetallic compounds can be obtained in the systems Li–*AE*–*Tt*(–N) (*AE* = Ca, Sr; *Tt* = Si, Ge, Sn, Pb). The obtained phases have a very similar composition and only quite subtle differences in the crystal structures with germanide or nitride ions providing a part of the anionic substructure, but occupying different crystallographic sites.

Results and Discussion

Synthesis

High temperature centrifugation aided filtration (HTCAF)[15,16] is a powerful tool to grow large single crystals of all phases $Li_{16}AE_6Tt_6N$ and $Li_{16}AE_6Tt_{6.5}$ (*AE* = Ca, Sr; *Tt* = Si, Ge, Sn, Pb), of which $Li_{16}Sr_6Ge_6N$ was investigated in detail.

The addition of sufficient amounts of nitrogen in the starting mixture in form of lithium nitride of alkaline-earth metal nitride leads to the formation of $Li_{16}AE_6Tt_6N$, while in absence or only small content of nitrides the ternary phases $Li_{16}AE_6Tt_{6.5}$ are obtained. Both types of phase yield very similar powder X-ray diffraction patterns, which can be indexed in a cubic system with smaller lattice parameters *a* and thus smaller cell volumes *V* indicating the formation of the nitride and larger unit cells for the pure tetrelides. However, higher values of *Tt* contents appear often to be associated with a certain amount of H incorporated in the structures.

Interestingly, the title phases are the dominating products in reaction mixtures containing Sr, while experiments with Ca or Ba as the alkaline-earth metal component under otherwise identical conditions rather lead to lithium alkaline-earth tetrelides of the type Li_2EATt.[10]

Table 1. Experimentally obtained phases in the systems $Li_{16}AE_6Tt_{6+x}N_{1-y}$ lattice parameters [Å] and crystal structure refinement method.

Phase	*a* [Å]	Refinement method
$Li_{16}Ca_6Si_{6.5}$	13.0892(5)	
$Li_{16}Sr_6Si_{6.5}$	13.4929(7)	
$Li_{16}Sr_6Ge_6N$	13.4775(2)	PXRD
$Li_{16}Sr_6Ge_{6.078(5)}N_{0.922(5)}$	13.4943(4)	ScXRD
$Li_{16}Sr_6Ge_{6.456(8)}$	13.5733(6)	ScXRD
$Li_{16}Sr_6Sn_6N$	14.0478(5)	
$Li_{16}Sr_6Sn_{6.5}$	14.1155(3)	
$Li_{16}Sr_6Pb_{6.73(5)}N_{0.36(10)}$	14.1685(4)	ScXRD

Although we did not study all possible combinations (Table 1), it is clear that the title compounds form with strontium and the tetrel elements *Tt* = Si, Ge, Sn Pb. In case of silicon, we additionally have strong evidence for the formation of the corresponding calcium compounds, although with calcium and barium the generation of lithium alkaline-earth metal tetrelides of the type Li_2EATt is strongly preferred.

It remains unclear, if hydride ions further stabilize the phases $Li_{16}Sr_6Tt_{6.5}$. According to DTA-TG-MS investigations, the amount of H is concomitantly increasing with an increasing content of *Tt*. However, only few samples revealed a significant hydrogen content in DTA-TG-MS measurements (see below). Additionally, neither the obtained hydrogen contents nor complete filling of the octahedral site would lead to a charge-balanced situation, an electronic excess still remains, in agreement with electric properties and electronic structure calculations as will be shown below.

Crystal structure

The title phases crystallize in an ordered defect-variant of the $Sc_{11}Ir_4$ type with selective occupation of the smaller octahedral voids in the origin (000) with N and the larger rhombic dodecahedral voids in ($00^1/_2$) with *Tt*. All crystal structures of the title phases can be derived from the $Sc_{11}Ir_4$ type according to Table 2.[17] Details on data collection and structure refinement are given in Tables 3 and S1, atomic coordinates, site occupancies, and thermal displacement parameters are given in Tables S2 and S3, and selected distances in Tables 4 and S4.

We first focus on the structure of idealized $Li_{16}Sr_6Ge_6N$. Here, all four sites with high multiplicities in the cubic intermetallic aristotype are fully occupied by Li (2×), Ge and Sr. Nitrogen is located in the special position 4*a* (000) in mutually isolated octahedra Sr_6N, while 4*b* ($00^1/_2$) remains empty. The germanide ions $Ge(1)^{4-}$ are coordinated by eight Li in a tetragonal prism, capped at all four trapezoid faces by Sr. In sum, the resulting coordination polyhedron is rather close to an icosahedron. The strontium ions interconnect the coordination polyhedra around Ge(1) to chains running parallel all three crystallographic axes, thus forming a framework in which the Sr_6N octahedra are embedded (see figure 1).

Lithium is located in two differently coordinated crystallographic sites. Li(1) is situated in an equilateral triangle from three $Ge(1)^{4-}$ ions, located only very slightly out of plane (0.125 Å). Li(2), however, in the ideal $Li_{16}Sr_6Ge_6N$ resides in a similar equilateral triangle from three $Ge(1)^{4-}$, but with 0.827 Å

Table 2. Relationship between $Sc_{11}Ir_4$, $Li_{16}Sr_6Ge_6N$ and $Li_{16}Sr_6Ge_{6.5}$ as well as related structure types in space group $Fm\bar{3}m$.

Site	4*a*	4*b*	24*d*	24*e*	32*f*	32*f*	Ref.
$Sc_{11}Ir_4$	Ir	Ir	Ir	Sc	Sc	Sc	[17]
$Er_3Pd_8Sb_4$	Sb	Sb	Sb	Er	Pd	Pd	[18]
$U_6Fe_{16}Si_7C$	C	Si	Si	U	Fe	Fe	[19]
Th_6Mn_{23}	–	Mn	Mn	Th	Mn	Mn	[20]
$Li_{16}Sr_6Ge_6N$	N	–	Ge(1)	Sr	Li	Li	
$Li_{16}Sr_6Ge_{6.5}$	–	$^1/_2$ Ge(2)	Ge(1)	Sr	Li	Li	

© 2022 The Authors. Zeitschrift für anorganische und allgemeine Chemie published by Wiley-VCH GmbH

Table 3. Selected information on crystal structure determination.

Composition	$Li_{16}Sr_6Ge_6N$	$Li_{16}Sr_6Ge_{6.078(1)}N_{0.922(5)}$	$Li_{16}Sr_6Ge_{6.456(8)}$	$Li_{16}Sr_6Pb_{6.78(5)}N_{0.36(10)}$
Refinement method, software	Powder Jana2006[21]	Single crystal SHELXL-2018[22–23]	Single crystal SHELXL-2018[22–23]	Single crystal SHELXL-2018[22–23]
Space group	$Fm\bar{3}m$ (No. 225)	$Fm\bar{3}m$ (No. 225)	$Fm\bar{3}m$ (No. 225)	$Fm\bar{3}m$ (No. 225)
a [Å]	13.47748(18)	13.4943(4)	13.5733(6)	14.1685(4)
V [Å^3]	2448.08(6)	2457.3(2)	2500.7(3)	2844.3(2)
Z	4	4	4	4
ρ_x [g cm^{-3}]	2.9474	2.948	2.938	4.777
$R1$, $wR2$ (all data)	0.027, 0.042	0.019, 0.031	0.028, 0.049	0.025, 0.046

Table 4. Selected interatomic distances in $Li_{16}Sr_6Ge_6N$ and $Li_{16}Sr_6Ge_{6.5}$ in [Å].

Distance	$Li_{16}Sr_6Ge_{6.078(5)}N_{0.922(5)}$	$Li_{16}Sr_6Ge_{6.456(8)}$
Sr(1)–N	2.676(1)	–
Sr(1)–Ge(1)	3.445(2) 4×	3.422(3) 4×
Sr(1)–Ge(2)	4.071(1)	3.835(22)
Sr(1a)–N	2.902(11)	–
Sr(1a)–Ge(1)	3.406(2) 4×	3.405(2) 4×
Sr(1a)–Ge(2)	3.845(11)	3.682(26)
Ge(1)–Li(1)	2.757(4) 4×	2.772(5) 4×
Ge(1)–Li(2)	2.876(4) 4×	2.900(7) 4×
Ge(1)–Sr(1a)	3.406(2) 4×	3.406(2) 4×
Ge(1)–Sr(1)	3.445(2) 4×	3.422(2) 4×
Ge(2)–Li(2)	–	3.060(7) 8×
Ge(2)–Sr(1a)	–	3.682(26) 6×
Ge(2)–Sr(1)	–	3.834(22) 6×

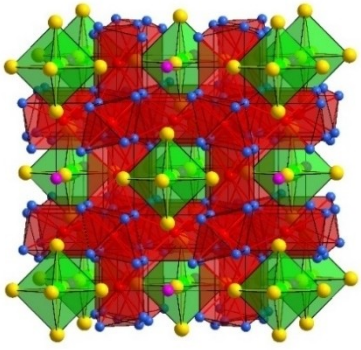

Figure 1. Extended unit cell of $Li_{16}Sr_6Ge_6N$. Sr_6N octahedra (small void, green, with yellow Sr at the vertices) are embedded in a framework of rhombic prisms $Ge(1)Li_8$ (red, with blue Li at the vertices). The large rhombic dodecahedral void in (00$^1/_2$) remains empty (pink, corresponds to Ge(2)).

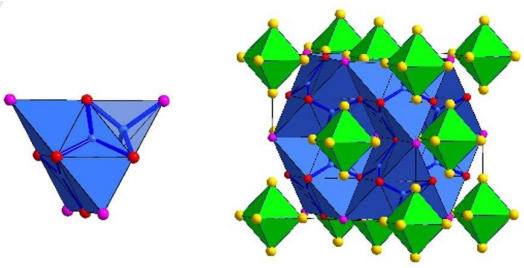

Figure 2. Left: Supertetrahedron $Li_8Ge(1)_6Ge(2)_4$ (with Ge(1) in red, Ge(2) in pink) The three-fold (Li(1)) and tetrahedral coordination (Li(2)) of the lithium ions (blue) is emphasized. Right: Arrangement of supertetrahedra $Li_8Ge(1)_6Ge(2)_4$ and octahedra Sr_6N (green, with yellow Sr at the vertices) in the crystal structure.

further out of plane. This triangle is completed to a tetrahedron when Ge(2) is present in $Li_{16}Sr_6Ge_{6.5}$, with Li(2) located nearly within the center. These two polyhedra are condensed to form supertetrahedra $Li_8Ge(1)_6Ge(2)_4$ (Figure 2). The center of such a supertetrahedron is located in ($^1/_4$ $^1/_4$ $^1/_4$), Li(1) and Li(2) form a stella quadrangula around this point.

Within this structure, the larger void in 4*b* (00$^1/_2$) can partially be occupied by some excess germanide ions, on cost of the occupation of the nitride site, providing the composition $Li_{16}Sr_6Ge_{6.5}$. This half-occupied site Ge(2) is coordinated by a cube of eight Li, capped at all quadratic faces by Sr and together realizing a rhombic dodecahedron (Figure 3).

With partial occupation of this site and depletion of the nitrogen site, the coordinating Sr realizes a split position. In the nitride Sr is surrounded by a quadratic pyramid $SrGe(1)_4N$ with the nitride ion at the apex and a very typical distance of 2.68 Å (e.g. 2.60 Å in $(Sr_6N)Ga_5$).[24] In presence of the Ge(2) the Sr is

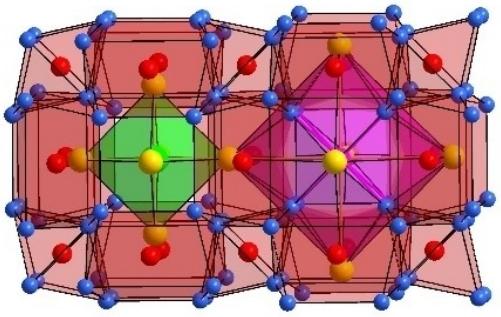

Figure 3. Small void (000) – octahedron (left, green) and large void (00$^1/_2$) – rhombic dodecahedron (right, pink) in the crystal structures of the title compounds. In $Li_{16}Sr_6Ge_6N$, the small void is fully occupied by N, whereas the large void remains empty. In $Li_{16}Sr_6Ge_{6.5}$, the small void is empty, while the larger void is partially occupied by Ge(2). Ge(1) in red, Ge(2) in pink, N in green and Li in blue.

© 2022 The Authors. Zeitschrift für anorganische und allgemeine Chemie published by Wiley-VCH GmbH

displaced about 0.20 Å towards the germanide ion, thus optimizing the distance from 3.83 Å to 3.68 Å. Again a quadratic pyramid $SrGe(1)_4Ge(2)$ is realized, now with Ge(2) at the apex. For comparison, the distances of Sr to the Ge(1) realizing the quadratic faces of the pyramids stay virtually identical with 3.45 Å in $Li_{16}Sr_6Ge_6N$ and 3.41 Å in $Li_{16}Sr_6Ge_{6.5}$ (Figure 4).

While refinements of occupancies in all other compounds are close to the idealized compositions $Li_{16}Sr_6Tt_6N$ and $Li_{16}Sr_6Tt_{6.5}$, only for the plumbide we encounter an enhanced occupation of the rhombic dodecahedral site with lead and some concomitant occupation of the octahedral void with nitrogen (see Table 3) close to the charge-balanced situation. This different behavior of the plumbide will require further investigations.

In general, all distances Li–N, *Ae*–N, Li–*Tt*, and *Ae*–*Tt* match well with the values observed in corresponding nitrides and tetrelides.

DTA-TG-MS

$Li_{16}Sr_6Ge_6N$ melts incongruently above 588(5) °C (onset temperature); up to this temperature no significant mass loss is measurable, as shown in Figure 5.

However, analysis of the gas phase by mass spectrometry over samples $Li_{16}Sr_6Ge_6N$ shows the release of small amounts of nitrogen above 620 °C and traces of hydrogen in the temperature range around 250 °C and above 650 °C; the small hump at 250 °C presumably originates from adhering contaminants. Different samples of slightly different composition and synthesis processes show small differences in their nitrogen and/or hydrogen contents as well as in the release temperature into the gas phase. Decomposition products of $Li_{16}Sr_6Ge_6N$ include SrGe, Li_2SrGe, and other phases in varying amounts.

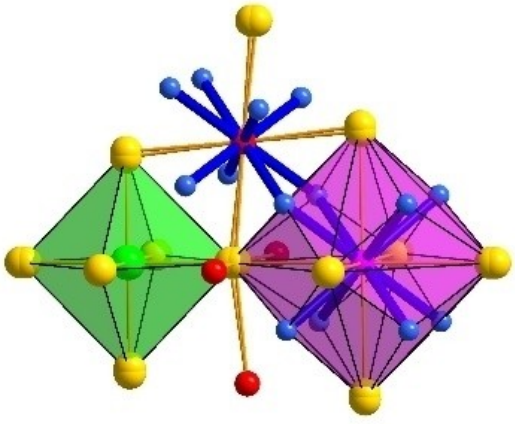

Figure 4. Coordination spheres of N (green), Ge(1) (red), and Ge(2) (pink) in the crystal structures of $Li_{16}Sr_6Ge_6N$ and $Li_{16}Sr_6Ge_{6.5}$. The split position Sr(1)/Sr(1a) (yellow) is emphasized. Blue spheres represent Li.

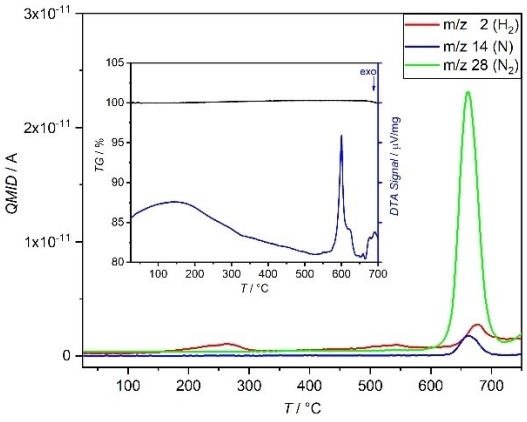

Figure 5. QMID (quasi multiple ion detection) current curve for release of hydrogen and nitrogen from $Li_{16}Sr_6Ge_6N$ upon heating. Inset: Simultaneous DTA signal and TG curve indicating melting with small weight loss at 588(5) °C.

Magnetic susceptibility

The magnetic susceptibility $\chi(T) = M/H$ of $Li_{16}Sr_6Ge_6N$ (Figure 6) was measured in the temperature range from 2 to 300 K in magnetic field of $\mu_0 H = 3.5$ T and 7 T. The susceptibility is negative and largely temperature-independent, except in the region below 40 K, where a Curie-type upturn is observed. The upturn originates very likely from paramagnetic impurities present in starting elements used for the synthesis. The room temperature susceptibility value amounts to $\chi \approx -2.8 \times 10^{-4}$ emu/mol. The value is the sum of the negative Larmor diamagnetic core susceptibility and two conduction electrons contributions – the positive Pauli paramagnetic spin susceptibility, and the negative Landau orbital diamagnetic susceptibility.

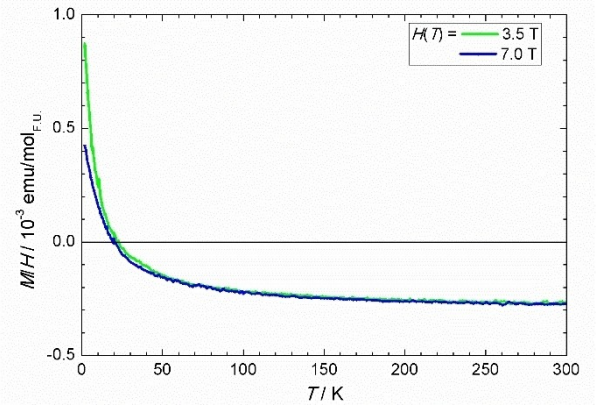

Figure 6. Magnetic susceptibility of $Li_{16}Sr_6Ge_6N$ measured in 3.5 T and 7 T magnetic field in the temperature range from 2 K to 300 K.

 © 2022 The Authors. Zeitschrift für anorganische und allgemeine Chemie published by Wiley-VCH GmbH

Electrical resistivity

The electrical resistivity $\rho(T)$ of $Li_{16}Sr_6Ge_6N$ and of $Li_{16}Sr_6Sn_{6.5}$ were measured in the temperature range from 3.8 to 300 K in zero magnetic field (Figure 7). The temperature dependence of both $Li_{16}Sr_6Ge_6N$ and $Li_{16}Sr_6Sn_{6.5}$ is metallic with positive temperature coefficient. For $Li_{16}Sr_6Ge_6N$, the residual resistivity value of $\rho(T) = 182\ \mu\Omega$ cm at 3.8 K indicates that the concentration of defects in the phase is moderate. The minimum around $T = 30$ K may be associated with magnetic impurities or grain boundary issues. The room temperature value $\rho(T) = 1066\ \mu\Omega$ cm indicates that $Li_{16}Sr_6Ge_6N$ is a moderate electrical conductor. In contrast, for $Li_{16}Sr_6Sn_{6.5}$ the small residual resistivity value at 2 K with $\rho(T) = 0.4\ \mu\Omega$ cm indicates that the concentration of defects in the phase is low, and the resistivity value $\rho(T) = 83\ \mu\Omega$ cm at 300 K is typical for metals, so $Li_{16}Sr_6Sn_{6.5}$ is a good electrical conductor. The high residual resistivity ratio of $Li_{16}Sr_6Sn_{6.5}$ (RRR ~ 207) indicates high purity of the sample, much higher than in $Li_{16}Sr_6Ge_6N$ (RRR ~ 5.9), which is similar to what is typically observed in polycrystalline samples.

Electronic structure and chemical bonding

The electronic densities of states (DOS) computed for $Li_{16}Sr_6T\tau_6N$ and $Li_{16}Sr_6T\tau_{6.5}$ with $T\tau$ = Ge, Sn, Pb are highly similar (Figure 8 and Figure S1). In $Li_{16}Sr_6Ge_6N$, the primitive unit cell contains one formula unit, which has 57 valence electrons. N 2*s* states are quite flat (no dispersion) and located at −11.4, −11.25 and −11.3 eV for $T\tau$ = Ge, Sn and Pb, respectively (not shown). The top region of the valence band has a width of about 3 eV, and it is separated by internal gaps of 4.0, 3.3 and 4.6 eV for $T\tau$ = Ge, Sn and Pb, respectively, from a group of states dominated by the $T\tau$ atom *s* orbital contributions. The top region can be divided into two energy ranges: (i) the lower part between −3.0 and about −0.25 eV contains contributions mainly from $T\tau$ *p*, N 2*p*, Sr 5*s*, 5*p* and 4*d*, Li 2*s* and 2*p*. (ii) the upper part between approximately −0.25 and 0 eV is a low DOS region yielding about 3.6 states per eV per formula unit for all $Li_{16}Sr_6T\tau_6N$. The integration of the total DOS over the upper part gives approximately 1 electron. Largely due to its abundant content, Li contributions appear to be dominant over both upper and lower parts, however in terms of per atom contributions, it is so only in the upper part. The corresponding electron energy dispersion curves are presented in Figure 9 and Figure S2. In all three nitrides, two bands cross the Fermi energy. The band with the higher energy forms a small electron pocket around the Gamma point with its minimum also at the Gamma point. The band with the lower energy has a saddle point near the L point very close to the Fermi energy. These two features are responsible for van Hove singularities in the vicinity of the Fermi energy. Their significance in relation to the physical properties will be the subject of further investigations.

The chemical bonding situation and charge transfer details were investigated only for $Li_{16}Sr_6Ge_6N$, since all three compounds have very similar electronic structures. The integration of the electron density (ED) inside the QTAIM basin (quantum theory of atoms in molecules) of an atom gives the number of electrons belonging to that atom and hence its effective charge. The numbers of excess electrons obtained for the anions are 1.90 and 2.87 for N and Ge, respectively. Sr atoms lose 1.16

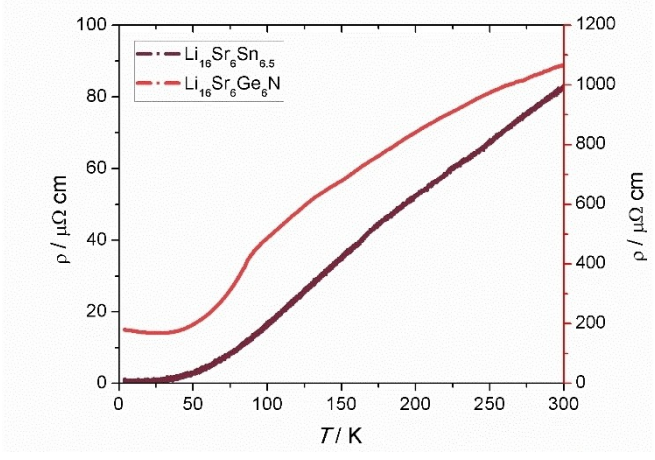

Figure 7. Electrical resistivity of $Li_{16}Sr_6Ge_6N$ (red) and $Li_{16}Sr_6Sn_{6.5}$ (black) measured between 3.8 and 300 K in zero magnetic field.

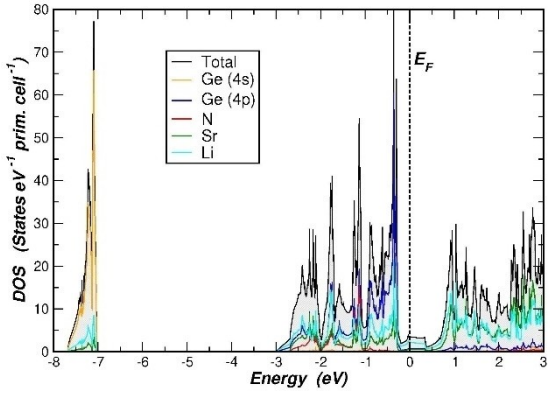

Figure 8. Electronic densities of states computed for $Li_{16}Sr_6Ge_6N$.

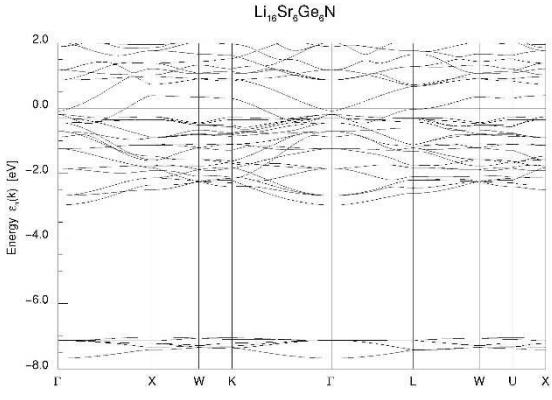

Figure 9. Electron energy bands computed along high symmetry lines in the Brillouin zone for $Li_{16}Sr_6Ge_6N$.

© 2022 The Authors. Zeitschrift für anorganische und allgemeine Chemie published by Wiley-VCH GmbH

electrons, while Li(1) and Li(2) donate 0.77 and 0.75 electrons, respectively. These effective charges already hint at the importance of ionic interactions for the cohesiveness of $Li_{16}Sr_6Ge_6N$. The topological analysis of the ELI-D distribution provides further information regarding the nature of bonding.

Before discussing the results of the ELI-D analysis, it is instructive to look at the structural aspects first. In the crystal structure the anions N and Ge are coordinated only with the cations, therefore no anion-anion covalent bonds are possible. The expectation would then be lone pair-like multi-atom bonds with the anions providing ~90% of the electrons inside the bond basins. The remaining ~10% come from the neighboring cations, 6 Sr atoms for the case of N, 4 Li(1), 4 Li(2) and 4 Sr atoms for the case of Ge. Formally, these bonds would have 8 electrons each. Because the formula unit contains one N and 6 Ge atoms, 56 valence electrons out of the 57 would be accounted for by these bonds. However, this line of reasoning cannot tell how the 57th electron will be distributed in the crystal structure. To answer this question, we should turn to ELI analysis.

The results of the topological analysis of the ELI-D field are in good agreement with the picture outlined above (Figure 10). The 7-atom N-(6×Sr) bond has 7.22 electrons of which 6.74 come from N and each Sr atom contributes 0.08. The Ge-based bond is technically a 13-atom cluster bond with 7.17 electrons provided by Ge, 0.06 by each Li and 0.12 by each Sr atom adding up to 8.14 bond electrons. The total electron count due to these bonds is 56.06, in perfect agreement with the expected value. The ELI-D attractors for the bonds that contain the remaining electron are located at the Wyckoff position 32 *f*: *x x x* with *x*~0.297. The bond population is only 0.02 electrons with contributions from 3 Ge (0.005 electron each) and 3 Li1 (0.001 electrons each) atoms. This means 0.16 electrons per formula unit, much smaller than the expected value of 1. The main reason for this is that the core basins of Li, N and Sr atoms actually contain slightly more than the according integer values, for example 2.05 and 2.14 for Li and N, respectively. As a result, there are fewer electrons in the valence region, 56.22 instead of 57. One of the attractors is shown in figure 10 by a small red ball. The attractor position lies in the plane formed by two Ge and two Li(1) atoms participating in the bond.

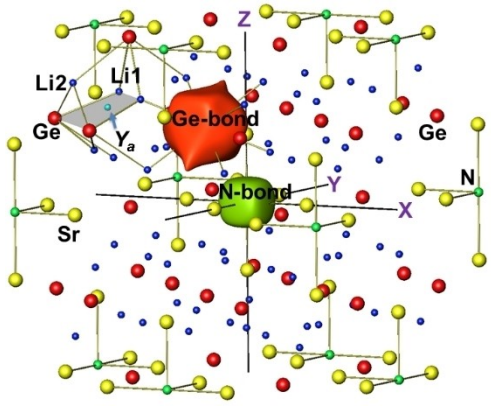

Figure 10. The ELI-D distribution with the isosurface value of 1.235 is shown around one Ge and one N atom. These regions encompass the attractors for the Ge- and N-centered 13- and 7-atom bonds, respectively. One particular location of the bond attractor corresponding to the 3×Ge-3×Li(1) bond is denoted by a small red ball and identified by Y_a. The coplanar arrangement of two Ge and two Li(1) atoms together with the attractor location is emphasized. Li atoms are blue, N green, Ge black and Sr yellow.

Conclusions

As we have shown earlier, the combination of lithium and calcium or barium with the tetrels leads to formation of rather simple intermetallic phases of the composition Li_2EaTt, even in presence of excess nitrogen. Upon substitution of the alkaline-earth metal by strontium, however, a much more complicated arrangement is realized. In presence of nitrogen, a smaller octahedral void is occupied by nitride ions in $Li_{16}Sr_6Tt_6N$. In absence of nitrogen a virtually identical framework of the metal ions results, but with further tetrelide ions located in a somewhat larger rhombic dedecahedral void, which is empty in the nitride, resulting in the composition $Li_{16}Sr_6Tt_{6.5}$. In both cases, metallic phases with excess electrons compared to a simple ionic description with only closed shell ions result, in well agreement to physical properties measurements and electronic structure calculations. Although in few samples the presence of small amounts of hydrogen was detected, but it content appears insufficient to lead to a charge balanced situation. The in-depth analysis of physical properties of the title phases is subject of ongoing investigations.

Experimental Section

Synthesis

In view of the sensitivity of the starting materials and the reaction products to moisture and air, all manipulations associated with sample preparation and handling were performed in inert atmosphere using an argon-filled (Praxair, >99.999%, purified with AirLiquide Oxisorb catalyst) glove box (Mbraun, $p(O_2)/p_0 < 0.1$ ppm, $p(H_2O)/p_0 < 0.1$ ppm).

Li_3N, Ca_3N_2, and Sr_2N as nitride precursors were synthesized from the elements (Li: Evochem, 99.9%; Ca: Alfa Aesar, distilled dendritic pieces, 99.98%; Sr: Alfa Aesar, distilled dendritic pieces, 99.95%) and nitrogen (Praxair, 99.999%, further purified by molecular sieve, 3 Å, Merck), the metallic elements were used without further purification.

Sample preparation was carried out employing a modified high temperature centrifugation-aided filtration (HTCAF) technique.[15–16] Large single crystals of the different specimens up to several mm in size were grown from mixtures of the elements or binary nitrides in the molar ratio of about Li:*Ae*:*Tt*:N = 5–20:0.5–2:1:0–2; the weight of the samples amounted to ~1 g. To synthesize nitrogen-free samples, no binary nitrides were added to the starting mixture. The materials were filled in a Ta ampoule equipped with a strainer, welded shut, and subsequently sealed in a quartz tube. The quartz tube was placed in a stainless-steel container fitted with quartz wool and put in a box furnace. The temperature program involved heating to 1023 K by 100 Kh^{-1}, annealing for 2 h and subsequent

 © 2022 The Authors. Zeitschrift für anorganische und allgemeine Chemie published by Wiley-VCH GmbH

cooling to 573 K for the Ca and 673 K for the Sr phases. After turning the stainless-steel container by 180°, the sample was centrifuged at 3000 min^{-1}, removing the flux consisting mostly of lithium, low melting binary phases, and further unspecified impurities. In this respect, Li functions thrice in this reaction as constituting agent, flux for crystal growth, and sink for excess nitrogen via formation of small amounts of Li_3N.

After opening the Ta tube in the glove box, agglomerates of blackish cubic crystals with a silver luster as well as smaller amounts of still unspecified phases were observed on the bottom of the ampoule. Li flux acts as a sink for excess nitrogen leading to varying amounts of reddish-black single crystals of Li_3N in the form of hexagonal platelets as a by-product; however, these crystals are easily sorted out considering morphology, color and electrical conductivity. Every selected crystal was checked by two-point resistivity measurement at ambient temperature to show high conductivity. Small amounts of hydrogen observed in the intermetallic phases obtained are due to H contamination in the lithium starting material. Presence of N in the starting mixture leads to preferential formation of the tetrelide-nitride phases.

X-ray diffraction data collection and refinement

Laboratory PXRD patterns of finely ground gray powder samples were collected on a Huber G670 imaging plate Guinier camera (CuKα1 radiation, $2\theta_{max} = 100°$, Huber Diffraktionstechnik GmbH & Co. KG, Rimsting, Germany). The powder samples were placed between Kapton films to prevent degradation in air. Rietveld refinements were performed using the Jana2006 program.[21]

Indexing of the PXRD pattern for a $Li_{16}Sr_6Ge_6N$ sample (Figure 11) readily yielded an F-centered cubic unit cell with $a = 13.4775(2)$ Å. Crystal structure solution was accomplished with the Superflip program implemented within the Jana2006 package. The derived model in space group *Fm*3*m* was completed by adding Li atoms revealed in the subsequent difference Fourier mapping. All atoms were eventually refined isotropically. The U_{iso} values for all Li positions were kept equal in the final cycles of the refinement.

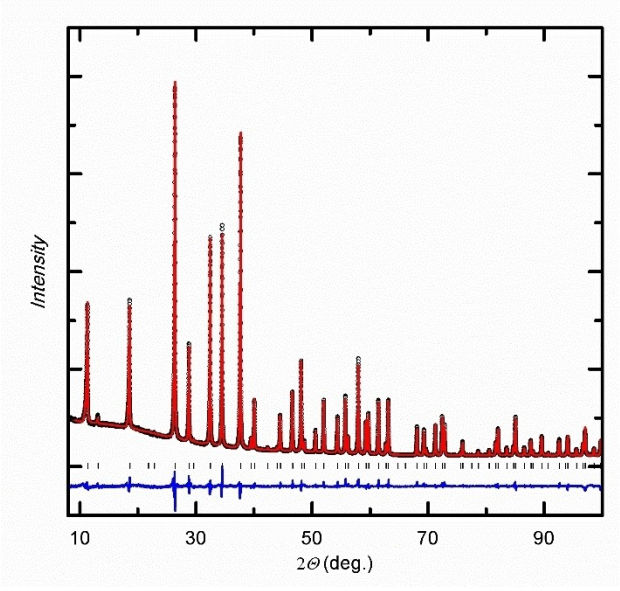

Figure 11. Powder X-ray diffraction pattern of a $Li_{16}Sr_6Ge_6N$ sample. Open circles denote the experimental data. The calculated profile and the difference curve are given in red and blue, respectively. Tick marks indicate the Bragg peak positions.

X-ray diffraction intensity data of single crystals sealed in glass capillaries were collected at room temperature on a Rigaku AFC7 equipped with a Saturn 724+ detector single crystal diffractometer using Mo$K\alpha_1$ radiation with a maximum 2ϑ of 70°. A numerical absorption correction was applied using the Xshape program followed by a crystal structure refinement with the Shelx software.[22,23] Crystallographic data, atomic coordinates, and isotropic displacement parameters from structure refinements obtained from single crystal X-ray diffraction data are summarized in Tables 1 and 2, relevant distances are listed in Table 3.

Further details of the crystal structure investigations may be obtained from FIZ Karlsruhe, 76344 Eggenstein-Leopoldshafen, Germany (fax: (+49)7247-808-666; e-mail: crysdata@fiz-karlsruhe.de, on quoting the deposition numbers CSD-2190983 (PXRD $Li_{16}Sr_6Ge_6N$), CSD-2192040 ($Li_{16}Sr_6Ge_{6.5}$), CSD-2192041 ($Li_{16}Sr_6Ge_6N$), and CSD-2192042 ($Li_{16}Sr_6Pb_{6.78(5)}N_{0.36(10)}$).

DTA/TG/MS measurements

The thermal behavior of selected samples of $Li_{16}Sr_6Tt_6N$ *and* $Li_{16}Sr_6Tt_{6.5}$ (Tt = Ge, Sn, Pb) was investigated using both a STA 449 C (NETZSCH) as well as by means of a TG-MS-system, which is a combination of a thermobalance STA 409 CD (NETZSCH) and a quadrupole mass spectrometer QMS 422 (Pfeiffer Vacuum). Both measuring systems are operated in the argon atmosphere of a glove box (MBraun).

The DTA-TG-measurements by means of the STA 449 C were performed in flowing argon atmosphere (Ar 99.999 % 100 ml/min with subsequent drying and oxygen post-purification via Big Oxygen Trap by Trigon Technologies).

The individual samples were measured under the following conditions – temperature range: 25 to 600–700 °C, sample mass: 7–50 mg, rate of heating and cooling: 5 K/min, crucible: tantalum DTA/TG crucible with perforated lid, thermocouple: type S (PtRh/Pt). The detected mass changes depending on temperature were subjected to buoyancy correction in accordance with the measurement conditions.

The characterization of the gaseous phase released during thermal decomposition was carried out using the TG-MS-system. The mass spectra were measured in a range $0 < m/z < 40$ and with 70 eV electron impact ionization. About 3–22 mg of the samples were weighed in a corundum Knudsen cell, covered by a lid featuring a small bore (0.3 mm), and transferred under protective conditions in the TG-MS-system. The samples were heated up to 750 °C with a heating rate of 5 K min. During the whole heat treatment, the gases evolving from the specimen intermixed with a continuous argon purging-gas stream and were directed to the ionization chamber of the mass spectrometer by using a skimmer located directly above the bore of the reaction crucible (Knudsen cell). Identification of the individual gas species was based on their isotopic patterns and mass-to-charge ratios of mother ions and fragments.

Magnetic susceptibility measurements

Magnetization data of polycrystalline aggregates of $Li_{16}Sr_6Ge_6N$ sealed in silica tubes (400 mbar He) were collected on a SQUID magnetometer (MPMS-XL7, Quantum Design) in the external fields of $\mu_0 H = 3.5$ and 7 T between 1.8 K and 300 K.

© 2022 The Authors. Zeitschrift für anorganische und allgemeine Chemie published by Wiley-VCH GmbH

Electric resistivity measurements

The resistivity of $Li_{16}Sr_6Ge_6N$ (polycrystalline agglomerates) and $Li_{16}Sr_6Sn_{6.5}$ (single crystals) were measured with a home-built resistivity equipment, which allows for samples to be handled in an inert atmosphere. The samples were contacted at four points using Ag paint and 25 μm thick Pt wires.

Computational Methods

First-principles electronic structure calculations were performed by using the all-electron, full-potential local orbital (FPLO) method.[26] Exchange-correlation effects were treated within the local density approximation as parametrized by Perdew and Wang.[27] Experimentally determined crystal structure data and Brillouin zone sampling with a grid of 24×24×24 were employed. Real space chemical bonding analysis in $Li_{16}Sr_6Ge_6N$ was carried out by applying the topological analysis of the electron density (ED)[28] and electron localizability indicator (ELI).[29] The ED, and ELI in the ELI-D representation[30–32] were calculated on a three dimensional, uniformly-spaced grid by a module implemented in the FPLO package.[33] The topological analysis was realized by the program Dgrid.[34] The basins of the ED are recognized as defining the atoms in a molecule or in a crystal structure in Bader's quantum theory of atoms in a molecule (QTAIM).[28] The ELI-D reveals the shell structure in free atoms by organizing the electrons with respect to the principal quantum number. In compounds, the ELI-D preserves the shell structure for the core electrons, and the features of the chemical bonding situation can be identified through the local maxima (attractors) of the ELI-D distribution in the valence region. The atoms participating in a bond can be determined by intersecting the according bond basin with the QTAIM atom basins.[35]

Acknowledgements

We thank Susann Scharsach for thermoanalytical measurements, Steffen Hückmann for powder X-ray diffraction data collection, Horst Borrmann for single crystal X-ray data collection, and Dominik Stoiber for additional synthetic and structural investigations supporting this study. Open Access funding enabled and organized by Projekt DEAL.

Conflict of Interest

The authors declare no conflict of interest.

Data Availability Statement

The data that support the findings of this study are available in the supplementary material of this article.

Keywords: Nitrides · Tetrelides · Crystal structure

[1] W. Schnick, H. Huppertz, *Chem. Eur. J.* **1997**, *3*, 679–683.
[2] T. Schlieper, W. Milius, W. Schnick, *Z. Anorg. Allg. Chem.* **1995**, *621*, 1380–1384.
[3] L. Link, R. Niewa, *Z. Anorg. Allg. Chem.* **2020**, *646*, 1105–1109.
[4] D. G. Park, Z. A. Gál, F. J. DiSalvo, *J. Solid State Chem.* **2003**, *172*, 166–170.
[5] L. Link, M. Pathak, F. Jach, P. Koželj, A. Ormeci, P. Höhn, R. Niewa, *Angew. Chem. Int. Ed.* **2021**, *60*, 7691–7696.
[6] S. J. Clarke, G. R. Kowach, F. J. DiSalvo, *Inorg. Chem.* **1996**, *35*, 7009–7012.
[7] N. S. P. Watney, Z. A. Gál, M. D. S. Webster, S. J. Clarke, *Chem. Commun.* **2005**, 4190–4192.
[8] F. Gäbler, M. Kirchner, W. Schnelle, M. Schmitt, H. Rosner, R. Niewa, *Z. Anorg. Allg. Chem.* **2005**, *631*, 397–402.
[9] M. Pathak, D. Stoiber, M. Bobnar, A. Ormeci, Yu. Prots, R. Niewa, P. Höhn, *Z. Anorg. Allg. Chem.* **2018**, *644*, 161–167.
[10] D. Stoiber, M. Bobnar, P. Höhn, R. Niewa, *Z. Naturforsch. B* **2017**, *72*, 847–853.
[11] R. U. Stelzer, Y. Ikeda, P. Srinivasan, T. S. Lehmann, B. Grabowski, R. Niewa, *J. Am. Chem. Soc.* **2022**, *144*, 7096–7110.
[12] H. Schäfer, B. Eisenmann, W. Müller, *Angew. Chem. Int. Ed.* **1973**, *12*, 694–712; *Angew. Chem.* **1973**, *85*, 742–760.
[13] B. Li, J. D. Corbett, *Inorg. Chem.* **2005**, *44*, 6515–6517.
[14] P. Höhn, G. Auffermann, R. Ramlau, H. Rosner, W. Schnelle, R. Kniep, *Angew. Chem.* **2006**, *45*, 6681–6685.
[15] M. Boström, S. Hovmöller, *J. Alloys Compd.* **2001**, *314*, 154–159.
[16] P. Höhn, J. T. Ballé, M. Fix, Yu. Prots, A. Jesche, *Inorganics* **2016**, *4*, 4040042.
[17] B. Chabot, K. Cenzual, E. Parthe, *Acta Crystallogr. Sect. B* **1980**, *36*, 7–11.
[18] M. Zelinska, S. Oryshchyn, C. Zhak, J. Y. Pivan, M. Potel, O. Tougait, H. Noel, D. Kaczorowski, *J. Solid State Chem.* **2010**, *183*, 2121–2126.
[19] D. Berthebaud, O. Tougait, M. Potel, E. B. Lopes, A. P. Gonçalves, H. Noël, *J. Solid State Chem.* **2007**, *180*, 2926–2932.
[20] J. V. Florio, R. E. Rundle, A. I. Snow, *Acta Crystallogr.* **1952**, *5*, 449–457.
[21] V. Petříček, M. Dušek, L. Palatinus, *Z. Kristallogr.* **2014**, *229*, 345–352.
[22] G. M. Sheldrick, *Acta Crystallogr. Sect. A* **2008**, *64*, 112–122.
[23] G. M. Sheldrick, *Acta Crystallogr. Sect. C* **2015**, *71*, 3–8.
[24] G. Cordier, M. Ludwig, D. Stahl, P. C. Schmidt, R. Kniep, *Angew. Chem. Int. Ed.* **1995**, *34*, 1761–1763; *Angew. Chem.* **1995**, *107*, 1879–1881.
[25] L. Palatinus, G. Chapuis, *J. Appl. Crystallogr.* **2007**, *40*, 786–790.
[26] K. Koepernik, H. Eschrig, *Phys. Rev. B* **1999**, *59*, 1743–1757.
[27] J. P. Perdew, Y. Wang, *Phys. Rev. B* **1992**, *45*, 13244–13249.
[28] R. F. W. Bader, in *Atoms in Molecules - A Quantum Theory, Vol. 22*, Clarendon Press, **1994**.
[29] Yu. Grin, A. Savin, B. Silvi, in *The Chemical Bond*, **2014**, pp. 345–382.
[30] M. Kohout, *Int. J. Quantum Chem.* **2004**, *97*, 651–658.
[31] M. Kohout, *Faraday Discuss.* **2007**, *135*, 43–54.
[32] F. R. Wagner, V. Bezugly, M. Kohout, Y. Grin, *Chem. Eur. J.* **2007**, *13*, 5724–5741.
[33] A. Ormeci, H. Rosner, F. R. Wagner, M. Kohout, Y. Grin, *J. Phys. Chem. A* **2006**, *110*, 1100–1105.
[34] M. Kohout, *DGRID*, 4.6, Radebeul, Germany, **2011**.
[35] S. Raub, G. Jansen, *Theor. Chem. Acc.* **2001**, *106*, 223–232.

Manuscript received: July 23, 2022
Revised manuscript received: August 22, 2022

 © 2022 The Authors. Zeitschrift für anorganische und allgemeine Chemie published by Wiley-VCH GmbH